A liquid-helium-cooled absolute reference cold load for long-wavelength radiometric calibration

Marc Bensadoun, Chris Witebsky, George Smoot, Giovanni De Amici, Al Kogut,[a] and Steve Levin[b]
Space Sciences Laboratory and Lawrence Berkeley Laboratory, University of California, Berkeley, California 94720

(Received 12 November 1990; accepted for publication 30 June 1992)

We describe a large (78 cm) diameter liquid-helium-cooled blackbody absolute reference cold load for the calibration of microwave radiometers. The load provides an absolute calibration near the liquid-helium (LHe) boiling point, with total uncertainty in the radiometric temperature of less than 30 mK over the 2.5–23-cm wavelength (12–1.3 GHz) operating range. Emission from those parts of the cold load not immersed in LHe is $\leqslant$25 mK and the reflection coefficient is $\leqslant 3.5\times 10^{-4}$. This cold load has been used at several wavelengths at the South Pole, Antarctica and at the White Mountain Research Station, California to calibrate spectral measurements of the cosmic microwave background radiation. For the instruments operated at 20-, 12-, 7.9-, and 4.0-cm wavelength at the South Pole, the total corrections to the LHe boiling-point temperature ($\sim$3.8 K) were 48 ± 23, 18 ± 10, 10 ± 18, and 15 ± 16 mK, respectively. In operation, the average LHe loss rate was $\leqslant$4.4 ℓ/h, allowing day-long periods of operation without a LHe fill. The boiloff rate is not strongly dependent on the radiative load at the aperture, yielding very stable operation and radiometric performance. Design considerations, radiometric and thermal performance, and operational aspects are discussed. A comparison with other LHe-cooled reference loads including the predecessor of this cold load is given.

I. INTRODUCTION

We have developed a large, liquid-helium-cooled cold load (CL) (Fig. 1) to permit precise absolute calibration for measurements of the long-wavelength ($\lambda\geqslant 1$ cm) spectrum of the cosmic microwave background (CMB). This instrument is based on one used for the same purpose in 1982–86,[1] with improvements derived from our previous experience.

This device has been used to make measurements of the CMB at wavelengths of 4.0, 7.9, 12, and 20 cm (7.5, 3.8, 2.5, and 1.5 GHz) in December 1989 from the South Pole and, at all but 12 cm, from the University of California's White Mountain Research Station in September 1988. The results of these measurements are reported by Kogut *et al.*,[2] De Amici *et al.*,[3] Sironi *et al.*,[4] Bensadoun *et al.*,[5] Levin *et al.*,[6] and De Amici *et al.*[7] Similar measurements at 7.9 and 12 cm have also been performed from White Mountain in past years using our previous load, providing a cross check of the accuracy of the calibration obtained with the load described here.

II. SCIENTIFIC CONTEXT

The CMB is a relic of the early, hot universe whose spectrum contains information on the evolution of the universe. Low-frequency measurements of the CMB have been made with microwave radiometers, devices whose output changes in proportion to the change in input power.[8] As described elsewhere,[1–9] the measurement consists of comparing the signal difference between the cold load and the sky.

The precision of the result depends upon the calibration: the most accurate measurement is achieved when the cold load characteristics are precisely known and closely matched to those of the sky, with impedance similar to that of free space for low reflection and a radiometric temperature close to that of the sky (4–10 K at $1<\lambda<30$ cm). The cold sky temperature requires an absorber immersed in liquid helium (LHe). Precise knowledge of the antenna temperature of the load requires low reflectivity, low emissivity of those parts not immersed in LHe, and precise knowledge of the physical temperature of the absorber.

Measurements of the CMB and tests for systematic effects are made from remote, high-altitude sites over a period of several days. Thus, the cold load must be transportable and robust, have stable performance and a low LHe loss rate, even during observations.

III. PREVIOUS COLD LOADS

Many long-wavelength measurements of the CMB have used LHe-cooled waveguide or coaxial cold loads to calibrate. Emission from the antenna and warm parts of such cold loads requires corrections of $\sim$2 K which have been a major source of error (at the $\pm$0.3-K level).[10–12] In the late 1960's, several measurements were made at centimeter wavelengths using LHe-cooled, quasi-free-space waveguide cold loads.[13–15] Uncertainty in the cold load

[a]Present address: Universities Space Research Association, Code 685.9, NASA Goddard Space Flight Center, Greenbelt, MD 20771.
[b]Present address: Jet Propulsion Laboratory, MS 169-506, Pasadena, CA 91109.

 0034-6748/92/104377-13$02.00

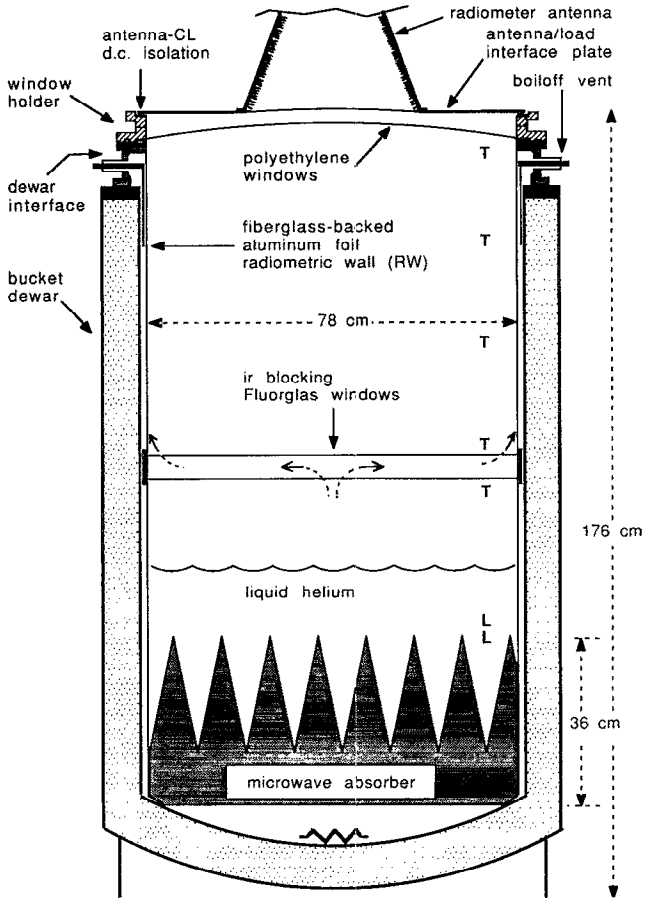

FIG. 1. Cross-sectional schematic of the cylindrical cold load. The He boiloff gas flows through holes in the IR-blocking windows (as indicated), then through the radiometric wall, up the annular space (not shown) and out the vents. The location of several of the discrete level sensors and temperature sensors are indicated by L and T, respectively. The resistive heater at the bottom of the CL is shown. The IR-blocking windows of the present load replace a manually operated shutter which was located just below the polyethylene windows of the 1982 load.

reference was reduced in these experiments to the ±0.1-K level, still a major source of error.

In 1982, the USA–Italy long-wavelength CMB collaboration built a large, quasi-free-space waveguide cold load[1,16] to eliminate the major sources of error present in previous cold loads over the band from 12–0.33 cm. The measurements produced by this collaboration[17] and continued in 1984–7 by the Berkeley group[4,18–20] using the 1982 load were the first for which absolute calibration error was insignificant over the range of 3–8-cm wavelength. The 1982 load performance at 12 cm (the design long-wavelength limit) limited the accuracy of the measurement at that wavelength.

The primary features of the 1982 cold load were (1) an absorber (Emerson & Cuming VHP-8 Eccosorb) immersed in LHe with reflection less than 2×10^{-4}, (2) an aluminum-coated (13 μm of aluminum) mylar radiometric wall with a diameter of 70 cm, (3) a low-emissivity, boiloff-cooled, manually operated shutter to reduce the heat leak between calibrations, (4) two 23-μm-thick polyethylene windows at the aperture to keep out air and moisture, and (5) an aluminum antenna/load interface plate. Insofar as they exist in the new load, these elements are indicated in Fig. 1; relevant dimensions are given in Table I.

TABLE I. Relevant geometrical and physical parameters of the 1988 cold load (described in this article) and the 1982 cold load (see Ref. 1 and Sec. II A).

Quantity	Dimension (cm) 1988 CL	1982 CL
Bucket dewar depth (at wall)	133	132
Bucket dewar i.d.	81.3	76.2
Radiometric wall (RW) i.d.	77.7	70
Distance from top of RW to top polyethylene window	0.5	0.5
Distance from top of RW to top Fluorglas window	74	...
Distance from top of RW to absorber tips	112	143
Distance from top of RW to absorber base	148	163
Separation of polyethylene windows (at edge)	3.8	15
Separation of IR-blocking windows	5.1	...
Height of absorber pyramids	25	15

In 1986, we made measurements at 21.3 cm, outside the nominal operating range of the cold load. We encountered radiometric problems with the absorber, which was too thin to give low reflection, and with the manually operated shutter near the top of the radiometric wall. During calibrations the shutter was opened to expose the absorber to the radiometer, but gaps between the shutter and the adjacent radiometric wall caused unacceptably high reflection and emission. Furthermore, the wall was aging and its emissivity may have degraded. The heat loads caused by the large antenna and the poor dewar vacuum made operations very difficult. Consequently, it was decided to build a new cold load with better thermal and operational characteristics, designed specifically for accurate long-wavelength measurements. The 1988 cold load, described in the present article, is similar in many respects to the 1982 load and draws extensively on the design, fabrication, operational experience as well as the radiometric performance of the previous effort.

IV. COLD LOAD DESIGN AND COMPONENT SELECTION

A. General description

The cold load consists of a bucket dewar with a microwave absorber immersed in a LHe bath (shown in Fig. 1; relevant parameters are given in Table I). A radiometric wall, an overmoded circular waveguide, extends from the LHe-temperature absorber to the ambient-temperature aperture, guiding the blackbody emission from the absorber up to the aperture to calibrate a microwave receiver. Each radiometer achieves a repeatable match to a flat interface plate covering the aperture, whose central hole matches the dimensions of the antenna mouth.

The temperature of the absorber, the dominant source of emission in the load (~99%), is determined from the

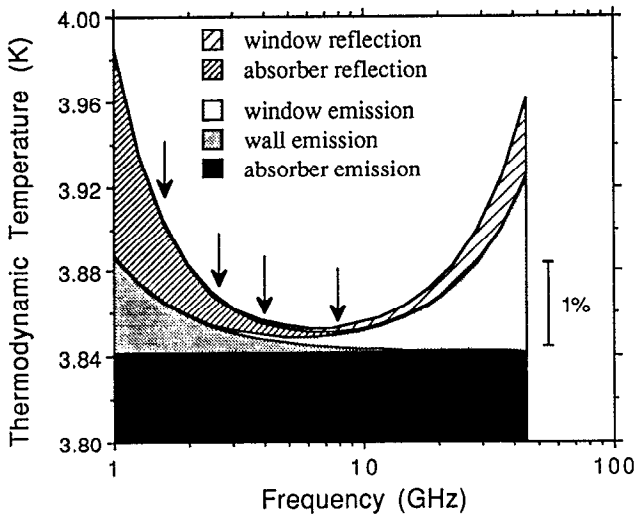

FIG. 2. Approximate contributions to the thermodynamic temperature of the cold load. Contributions due to reflection and wall emission depend on the specific properties of the radiometer observing the load. 1% of the total load signal is indicated on the right. Four arrows at 1.47, 2.5, 3.8, and 7.5 GHz (20-, 12-, 7.9-, and 4.0-cm wavelength) indicate the frequencies of the four radiometers which calibrated with the load at the South Pole in 1989. The window performance limits the high-frequency performance of the load while the absorber and wall emission limit the low-frequency performance of the load.

absolute pressure over the bath of boiling LHe. We compute the radiometric temperature of the load by adding the absorber's blackbody signal to the emission from the warm surfaces, windows, and joints in the load, and correcting for the effect of reflections from the load. Reflection of the signal broadcast by the radiometer and the signal from the absorber occurs at the interface plate, the windows, the helium liquid/gas interface, the absorber tips, and the absorber backing. These contributions to the cold load thermodynamic temperature are shown schematically for a typical radiometer in Fig. 2.

Thin polyethylene windows at the aperture prevent condensation of air and moisture inside the load. Infrared-blocking windows located just above the LHe bath intercept ~95% of the large IR heat load entering the aperture. Cold He boiloff gas is flowed past them to remove the absorbed heat from the load. To further reduce the radiative heat leak and protect the load during periods between calibrations, a low-emissivity, thermally insulated cover is placed over the aperture.

The LHe level, pressures throughout the load, and the temperatures of the absorber, the IR-blocking windows and the radiometric wall are critical to the evaluation of the cold load radiometric temperature and to the smooth operation of the load. Sensors to measure these quantities are located in the 1.6-cm annular space outside of the radiometric wall. A liquid-nitrogen level sensing system is also included for use during precooling and radiometric testing.

B. Physical description

The aluminum/fiberglass vapor-cooled LHe bucket dewar, manufactured by Kadel Engineering, has a neck tube consisting of two 57-cm-long, 1.6-cm-thick epoxy-fiberglass sections, with a He diffusion barrier of stainless-steel foil. The vacuum space has 225 g of activated charcoal getter material attached to the aluminum inner curvature head. The load weighs ~350 kg.

The polyethylene windows are sealed to the top and bottom of an annular aluminum holder. The window holder makes an O-ring seal with the top of the dewar interface. The dewar interface houses the electrical and pressure-sensor feedthroughs as well as the vacuum-insulated fill line, gas purge line, and vent lines.

The top of the radiometric wall attaches to the dewar interface. The upper and lower wall sections are joined by a three-ring aluminum annulus which also holds the IR-blocking windows. The foam absorber, backed by copper screen, is held in place by a friction fit with the wall and by contact with the bottom of the dewar. All seals are made gas-tight with O rings, silicone (for permanent seals), or latex (for the polyethylene windows). The fill line extends to the bottom of the inner curvature head.

C. The absorber

The absorber is characterized by its thermodynamic temperature ($\approx$4 K) and its reflectivity at that temperature and at the wavelengths of interest. The temperature of the LHe bath is reliably determined to $\pm$2 mK by measurement of the pressure over the LHe bath, with a cross check from electronic temperature sensors.

The absorber is constructed from VHP-12 Eccosorb[21] with a 5.7-cm backing layer of Eccosorb LS-22 and LS-24. This absorber is a carbon-impregnated, open-cell, urethane foam with good microwave absorption at 4 K, small volume, low specific heat, good porosity, and low cost.

Reflection from the absorber occurs at the front surface due to the imperfect dielectric matching of the pyramids to the LHe bath, and at the metal backing. The magnitude of the reflection is determined by the shape of the front of the absorber and the temperature- and frequency-dependent complex dielectric constant. As the absorber cools from 300 to 4 K, reflection from the front surface decreases slightly because the loss of the material decreases with temperature.

Power entering the absorber is attenuated twice, once before reflection and once afterward. The power emerging from the absorber is attenuated by a factor $\exp(-2\alpha t)$, where t is the absorber's effective thickness and α is its power-loss factor (or attenuation coefficient), given by

$$\alpha=\frac{2\pi}{\lambda}\sqrt{2\epsilon}\left[\sqrt{1+\tan\delta^2}-1\right]^{1/2}, \tag{1}$$

where ϵ is the real part of the dielectric constant and $\tan\delta$ is the loss tangent (the ratio of the imaginary and real parts of the dielectric constant).[22] In general, the dielectric constant is frequency dependent. The manufacturer's ϵ and $\tan\delta$ data for Eccosorb LS absorber show that $\alpha\propto\lambda^{-1}$ in the 10–30-cm wavelength region. While no such data are available for the VHP absorber, we expect it to behave similar to the LS absorber.

TABLE II. Contributions to the reflection coefficient r^2. The effect of the smaller antenna apertures is taken into account by the dilution factor, D (see Appendix A and Table IX). The position-dependent coherent reflection (0.7 times the sum of the reflections dependent on antenna position) predicts the amplitude of the sinusoidal variation in output obtained by varying the antenna/load separation (see Table V). The amplitude of the coherent reflection independent of antenna position is quoted (the phase of this term is unknown). To get reflected signal in K, multiply by $T_R T_{abs}$ from Table IX.

Source	Error in source	Reflectivity 20 cm (10^{-5})	12 cm (10^{-5})	7.9 cm (10^{-5})	4.0 cm (10^{-5})
Polyethylene windows power reflection ($2r_P^2$)	±10%	0.041	0.11	0.26	1.0
IR-blocking windows power reflection ($r_{F1}^2 D_F + r_{F2}^2 D_F$)	±100%	0.96	4.1	4.4	2.9
Liquid helium power reflection ($r_H^2 D_H$)	±1%	11	11	2.5	0.54
Absorber power reflection ($r_A^2 D_H$)	±50%	35	10	0.92	0.050
Position-independent coherent reflection (amplitude of sine curve)	±71%	24	15	3.6	0.68
Position-dependent coherent reflection (amplitude of sine curve)	±71%	16	17	20	4.5

The measured upper limit on the reflectivity of the 1982 load (VHP-8 absorber at 4 K) at $\lambda_0 = 12$ cm is $r_0^2 \leqslant 2 \times 10^{-4}$.[23] To obtain approximately the same upper limit at $\lambda = 23$ cm, the product of αt must be kept constant, so the absorber thickness has been increased by a factor of $\alpha(12\text{ cm})/\alpha(23\text{ cm}) = \lambda/\lambda_0 \approx 2$. The reflection for the four radiometers used at the South Pole in December 1989 is given in Table II.

D. Windows

The reflection, r, of a window of thickness $t \ll \lambda$ is[24]

$$r = \pi(\epsilon - 1)t/\lambda. \tag{2}$$

From Eq. (1), the emissivity, e, of a low-loss ($\alpha t \ll 1$; $\tan\delta \ll 1$) window is

$$e \equiv 1 - \exp(-\alpha t) \approx \alpha t = 2\pi t/\lambda \tan\delta \epsilon^{1/2}. \tag{3}$$

The reflected power (in units of antenna temperature) is the product of the power reflection coefficient, r^2, and the incident signal. The emitted power is e times the window's physical temperature. The dependence of both reflection and emission on thickness make thin windows desirable. Window reflection and emission increase at short wavelengths, setting the short-wavelength operating limit of the cold load. Reflection properties of the windows are given in Table II. The window material properties, emissivity, and emission are given in Tables III and IV.

The two 23-μm-thick polyethylene windows have low microwave reflection and emissivity, and enough strength to support a 4-Torr pressure differential and withstand mild physical abrasion at temperatures as low as 200 K. Warmed boiloff He gas circulates between the windows to maintain the top window at a temperature high enough to prevent condensation.

A 250-K blackbody filling the aperture of the load would radiate 106 W to the LHe bath. If this heat were allowed to reach the bath, it would result in an unacceptable LHe loss rate of 150 ℓ/h. We use two windows made from Fluorglas[25] 381-3 cloth just above the LHe bath to reduce the radiative heat leak. This FEP Teflon[26]-impregnated glass cloth exploits the high opacity of glass in the IR, the microwave transparency of both glass and Teflon, and the outstanding flexibility and durability of Teflon at cryogenic temperatures. The top window consists of one sheet, the bottom consists of two sheets. The material is 30% glass (dielectric constant $\epsilon_G \approx 5.0$) by volume with a total density of 0.0146 g cm^{-2} and a nominal thickness of ~ 75 μm. We model the Fluorglas material as a composite

TABLE III. Window material properties and emissivity. Emissivities are for the indicated thickness of material at each wavelength. The absorption coefficient, α, for glass is from extrapolation of published data and measured values. The data for glass at 290 K give upper limits on the emissivity at lower temperature. The error on the polyethylene and glass emissivities are ±33% and ±50%, respectively.

Material	Material properties ϵ	$\tan\delta$ (10^{-4})	α (cm^{-1}) (10^{-4})	t (μm)	Emissivity 20 cm (10^{-6})	12 cm (10^{-6})	7.9 cm (10^{-6})	4.0 cm (10^{-6})
Polyethylene	2.26	3 to 6		23	0.49	0.81	1.2	2.4
TFE Teflon	2.08	4		25	0.46	0.77	1.2	2.3
Glass (290 K)	5.9		7.1	50	3.6			
	5.9		16	50		8.1		
	5.9		31	50			16	
	5.9		93	50				47

TABLE IV. Emission from the windows and radiometric wall. Emissivity data are from Table III. Fluorglas emission is for 50 μm of glass and 25 μm FEP Teflon per layer. Wall emission is from a mode loss calculation at $\lambda=20$ cm, and from beam integration at $\lambda=7.9$ and 4.0 cm; the value at $\lambda=12$ cm is interpolated. The contribution from joints is listed separately.

Source	Physical temperature (K)	Emission 20 cm (mK)	12 cm (mK)	7.9 cm (mK)	4.0 cm (mK)
Polyethylene windows	250± 10	0.3±0.1	0.4±0.1	0.6±0.2	1.2±0.5
Upper IR-blocking window	50± 10	0.2±0.1	0.4±0.2	0.8±0.3	2.2±0.9
Lower IR-blocking window	25± 10	0.2±0.1	0.4±0.3	0.8±0.3	2.2±1.3
Wall (w/out joints)	4-250	4±4	2±2	0±1	0±1
Wall joints	30-250	13±13	7±7	2±2	2±2
Absorber leakage	20±10	7±7	0.7±0.8	0	0
Total emission		25±16	11±7	5±3	8±3

with dielectric constant $\epsilon_F=\epsilon_T(1-\phi)+\epsilon_G\phi\approx 3.0$, where ϵ_T is the dielectric constant of Teflon and ϕ is the fraction of glass by volume. The 381-3 fabric is inexpensive, easy to handle, and available in wide rolls (92 cm). The heat absorbed by these windows is removed from the load by cold He boiloff gas circulating between the windows and then out of the load. No correction to the reflection or emission is made for the small solid angle subtended by the vent holes in these windows (see Sec. IV F).

E. Radiometric wall

We used two identical 77.7-cm i.d., 1-mm-thick epoxy-fiberglass cylinders with 1100-H19 aluminum 25-μm thick (10 skin depths at 1.5 GHz) on the inner surface, leaving a clearance of $\sim$1.6 cm between the radiometric wall and dewar wall. The smooth, low emissivity wall subtends a small gain-weighted solid angle. Its thermal conductivity is low, and heat conducted down the wall is removed by boiloff gas.

Radiometric wall emission received by the radiometer depends on the measured temperature profile of the wall, the surface resistivity, the antenna beam pattern (or field configuration), and the effect of small gaps in the wall. The surface resistivity, R_s, is[27]

$$R_s=\sqrt{\frac{\pi c\mu}{\lambda\sigma}}\ \Omega, \tag{4}$$

where $\mu=4\pi\times10^{-7}$ (H/m) and σ is the conductivity (Ω^{-1}/m). The emissivity of the surface is $R_s/c\mu$, proportional to $\lambda^{-1/2}$. At $\lambda=20$ cm, the wall emissivity varies from 3×10^{-5} at 273 K to 1×10^{-5} in LHe, where the conductivity is determined from the Gruneisen relation.[28] Emission from a 2.5-μm-thick waxy dielectric coating is included, but contributes negligibly.

Below the IR-blocking windows, a small hole in the wall allows for measurement of the pressure over the LHe bath. 32 holes, spaced evenly around the circumference 4 cm above the top IR-blocking window, allow the He boiloff gas to exit the radiometric space. Each hole is 6.4 mm in diameter and backed by copper mesh. Close to the top of the upper wall section are holes for pressure sensing and gas purging.

Small steps in the radiometric wall diameter at the joints between the fiberglass sections and the window holders cause a small impedance change. The step sizes average $\leqslant$0.5 mm (and never exceed 1 mm). A 0.5-mm-thick epoxy-fiberglass layer at the aperture joint electrically isolates the load from the radiometer interface plate to eliminate ground loops or eddy currents. The leakage and reflection from the joints are expected to be minimal.

F. Boiloff helium flow and heat flow

The gas flow serves the dual purpose of removing the 50–100-W radiative heat load and cooling the electrical leads, plumbing, and the radiometric and dewar walls. The gas flow is channeled up through holes in the middle of the lower IR-blocking window and out along the outer edge of the upper window to remove the radiative heat load, then immediately through the vent holes in the radiometric wall and up the annular space between it and the dewar wall (see Fig. 1). The IR-blocking window venting cross section (16 cm^2 for each window) is larger than the wall vent cross section (10 cm^2) to prevent any significant flexing of the windows. The boiloff gas exits the annular space through six vents near the aperture; a small fraction is heated and circulated between the polyethylene windows, while the remainder is vented to the atmosphere $\sim$3 m away.

G. Sensors and heaters

A four-wire superconducting sensor (AMI 60 cm) measures the LHe level and a capacitive sensor (Cryomagnetics Model 50) measures the liquid-nitrogen level. In addition, ten 330-Ω Allen–Bradley carbon resistors indicate reliably whether the liquid level is above or below each of them, allowing calibration of the continuous sensors and providing a backup system. The resistor insulation is removed to improve the thermal contact with their surroundings. Operated at a 10-V bias to provide self-heating, their current typically changes from 5 mA in LHe to 9 mA in cold He gas, and from 24 mA in liquid nitrogen to 27 mA in cold nitrogen gas. The resistors respond to $\sim$1 mm changes in the cryogen level when at the liquid surface. The discrete sensors are located in the curvature head, at intervals along the lower portion of the wall, and at, and

just above, the absorber tips. The resistors and the LHe continuous sensor are protected from splashing cryogen to improve their stability and reliability.

Pressures inside the load are measured via small tubes leading out to differential pressure gauges. The differential pressures across the windows and wall (important because the cryogen level sensors are outside of the wall) are measured to $< \pm 0.2$ Torr. The differential pressure over the cryogen (compared to ambient) is also measured to $< \pm 0.2$ Torr.

The absorber temperature is measured directly by two Lakeshore CGR-1500 carbon-glass resistors (CGR) and one 1N4148 diode. The CGRs have high sensitivity at LHe temperatures and are repeatable, capable of a ± 5-mK measurement, while the diode has better sensitivity at warmer temperatures. The radiometric wall temperature is measured to ± 5 K by six matched 1N4148 diodes epoxied to the exterior of the wall (one below the IR-blocking windows, five above). All of the sensors are located in the space between the dewar and radiometric walls. A 150-W heater at the bottom of the dewar aids in the removal of water vapor before precooling and liquid-nitrogen residue afterward, and in warming up the load. The dewar heater and the He gas heater are electrically isolated from the load.

V. RADIOMETRIC MODELING

We have modeled the radiometer-cold load system as a radiometer observing an ideal absorber, separated by a two-port device with power reflection r^2 and loss A. The load antenna temperature, $T_{A,\mathrm{CL}}$, is to first order the antenna temperature of the absorber, $T_{A,\mathrm{abs}}$. Corrections to $T_{A,\mathrm{abs}}$ are due to the reflection and absorption losses as the absorber signal propagates to the receiver, the power emitted from the lossy parts, and the power emitted by the radiometer which is reflected back to the radiometer. By design, the reflection and attenuation are small ($< 10^{-3}$) and the emission and reflection terms can be considered independently:

$$T_{A,\mathrm{CL}} = T_{A,\mathrm{abs}} + r^2(T_B - T_{A,\mathrm{abs}}) + A(T_{\mathrm{CL}} - T_{A,\mathrm{abs}}), \qquad (5)$$

where T_{CL} is the effective physical temperature of the lossy part, and T_B is the broadcast temperature of the radiometer.

The correction due to loss is the sum of the emissions from the windows and radiometric wall. To find the correction due to reflection we compute r^2 (where by r^2 we mean $|r|^2$ since, in general, r is complex) using the reflection properties of the antenna/load interface, the windows, the liquid-helium bath, the absorber, and the radiometer. The computation of r^2 is done in Appendix A.

This method of modeling the reflection gives the coherent (phase-dependent) reflection and the incoherent (phase-independent) reflection. Coherent reflection terms arise because the coherence length of the broadcast radiation is comparable to the separation between the sources of reflection. Incident monochromatic radiation, with amplitude E_0, reflecting off two sources, with amplitude reflection coefficients r_1 and r_2, gives rise to reflected radiation with amplitude $E_r = E_0 r_1 + E_0 r_2 e^{i\Delta\phi}$, where $\Delta\phi$ is the phase difference of the two signals when they are detected. The reflected power is given by

$$|E_r|^2 = E_0^2 r_1^2 + E_0^2 r_2^2 + E_0^2 r_1 r_2 \cos(\Delta\phi). \qquad (6)$$

The first two terms are independent of the phase of the signals and depend on the power reflection coefficients which are small (e.g., for the absorber, $r^2 \leqslant 3.5 \times 10^{-4}$). The last term, the coherent reflection term, depends on the phase difference and the *amplitude* reflection coefficients.

If one of the reflections is the reflection internal to the antenna, r_R, then the term depends on the position of the antenna and the term can be more than a factor of ten larger than other reflections in the load (r_R, typically ~ 0.1, is the largest reflection coefficient in the antenna/load system). If the separation between the two reflections is comparable to, or greater than, the coherence length of the signal (typically ~ 150 cm), the coherent reflection term is diminished. For terms involving significant reflections within the load (those from the IR-blocking windows, the helium interface, and the absorber) the separation is small ($\leqslant 40$ cm) compared to the coherence length. Radiometer reflection r_R occurs far (~ 150 cm) from the significant reflections in the load and so terms involving r_R are reduced to a level comparable in magnitude to the coherent terms involving only reflections inside the load.

VI. MEASUREMENT OF RADIOMETRIC PROPERTIES

Our past measurements of the polyethylene window emission and reflection are in agreement with the theory (see Sec. IV D) using the parameters listed in Table III. The polyethylene window reflection and emission are given in Tables II and IV.

A. Cold load reflection

We measured the reflection of the antenna/cold load system at 20-cm wavelength. At $\lambda = 20$ cm, reflection from the absorber, r_A, and radiometer, r_R, are the dominant sources of reflection in the load, so that, neglecting coherent reflection, $r^2 \sim r_R^2 + r_A^2$ (see Table II). Figure 3 shows slotted-line measurements of the reflection with the antenna viewing the absorber at ambient and LHe temperatures. No change in the total reflection between ambient temperature and 4 K is observed at the level of the noise in the data (± 2 dB). The average of the measured reflection over the bandwidth of the radiometer is 3.5×10^{-4} (with $\pm 50\%$ error), consistent with the absorber reflection upper limit specified by the manufacturer (see Fig. 4).

Direct measurements of the cold load or absorber reflectivity were not made at shorter wavelengths. We use the estimated upper limit on absorber reflection as a function of frequency from the manufacturer's specifications (see Fig. 4) to scale from the value measured at 20-cm wavelength, with an uncertainty of $\pm 50\%$ from the 20-cm datum. Values for the radiometers used at the South Pole are given in Table II.

We have determined the reflection correction to the absorber temperature when the antenna views the load.

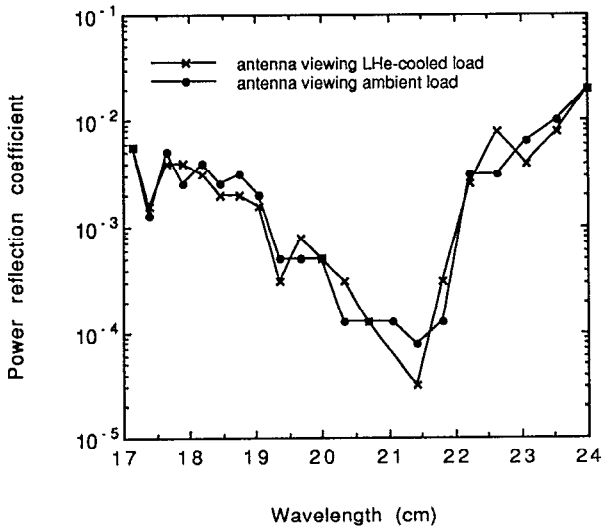

FIG. 3. Reflection measured with the 20-cm wavelength radiometer. (a) Comparison of the total (antenna and load) reflection with the antenna observing the absorber at ambient and LHe temperatures. The measurement was made with a slotted line inserted between the radiometer antenna and waveguide-coaxial transition.

However, signal is reflected even when the antenna observes the sky. What is important for the CMB measurement is the difference in the cold load and sky reflection corrections. Because the cold load reflection coefficient is small (see Tables II and VI) and the antenna/load interface reflection is small (see Appendix B), we expect this difference also to be small.

B. Infrared-blocking windows

We measured the emission from ambient temperature Fluorglas 381-3 material at 20, 7.9, 4.0, 3.0, and 0.33 cm by

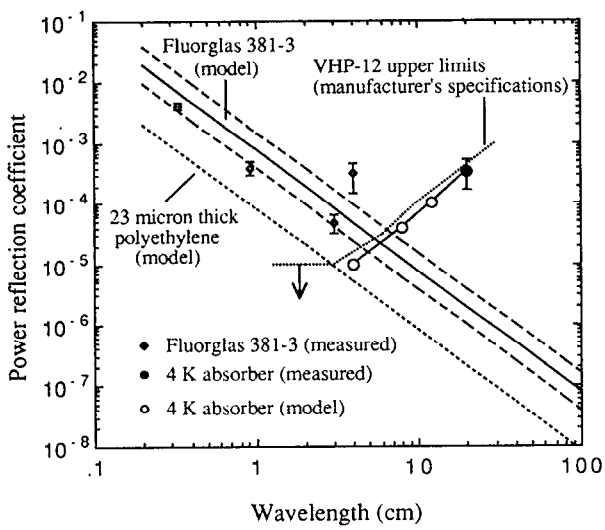

FIG. 4. Absorber and window power reflection coefficients. The absorber used has additional backing to give lower reflection than the manufacturer's specified upper limit for Eccosorb VHP-12. The value at 20 cm is from the measurement in Fig. 3. Measured values are shown for a single thickness (68 μm) of the Fluorglas IR-blocking window material and the model (the value used in the analysis) is the average of the theoretically predicted value and the measured value at 0.91-cm wavelength. The uncertainty used for the Fluorglas reflection is indicated. Reflection from a single layer of 23-μm polyethylene is shown.

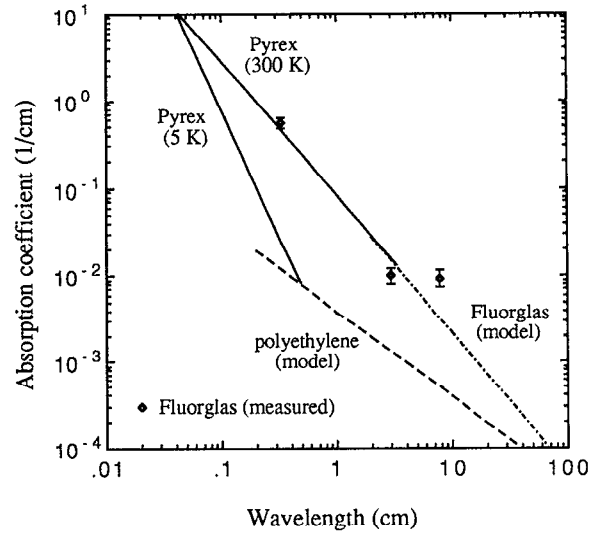

FIG. 5. Absorption coefficient of Fluorglas material. The radiometer data agree with the Pyrex data for $0.03 < \lambda < 0.3$ of Halpern *et al.* and their best fit parameters are used with an uncertainty of $\pm 50\%$ as indicated on the long-wavelength extrapolation. This uncertainty allows for a decrease in the absorption as the Fluorglas material cools.

measuring the change in the signal when the material was placed on an aluminum sheet which reflected the radiometer beam to the sky (a stable cold reference). The measured absorption coefficient in the 20–0.33-cm range is in good agreement with published sub-mm spectrometer measurements of Pyrex over the 0.5–0.033-cm range[29] (see Fig. 5). The measured absorption is significantly lower at 5 K that at room temperature at wavelengths longer than 0.05 cm. We use the room-temperature spectrometer data extrapolated to cm wavelengths (with an uncertainty of $\pm 50\%$ to account for errors in the extrapolation) to model Fluorglas absorption (see Table III).

We determined the reflection coefficient at 4.0-, 3.0-, and 0.33-cm wavelength by measuring the combined emission and reflection, then removing the emission and coherent reflection signals. We measured the combined reflection and emission by measuring the change in signal when the Fluorglas was placed over the mouth of an upward-pointing antenna. Additional measurements at $\lambda = 0.91$ cm with a slotted-line reflectometer yielded a Fluorglas power reflectivity of $(4 \pm 1) \times 10^{-4}$. The measured values are shown in Fig. 4. The line in Fig. 4 is the average of the reflection from Eq. (2) and from the measurement at 0.91 cm. The other measured values lie within a factor of 2 of this line and we take the error to be $+100\%/-50\%$. Table II shows the IR-blocking window reflection for the radiometers used at the South Pole.

C. Reflection dependent on antenna position

Table II gives the calculated power-reflection coefficient of the position-dependent coherent reflection signal for the four instruments which used this load to calibrate at the South Pole in 1989 (see Appendix A for derivation). The position-dependent signal is that part of the coherent reflection signal which varies with the antenna/load sepa-

TABLE V. Coherent reflection test summary. The predicted amplitude is from Table II and Table IX; the uncertainty is $+100\%/-50\%$, arising from the uncertainty in r_R. All measurements give only upper limits on the effect; the 1σ limit is shown. No measurement was made at 12-cm wavelength.

	Amplitude of effect (mK)			
	20 cm	12 cm	7.9 cm	4.0 cm
Predicted	8	5	18	13
Measured	<14	···	<30	<21

ration. To measure this effect, an extension to the radiometric wall is placed at the load aperture to allow the antenna to move vertically by $\lambda/2$ and map out at least one period of the expected sine curve. Tests at 20-, 7.9-, and 4.0-cm wavelengths show no sine curves within the limits of the signal noise. The measured upper limits on the amplitude are consistent with theoretical predictions (see Table V).

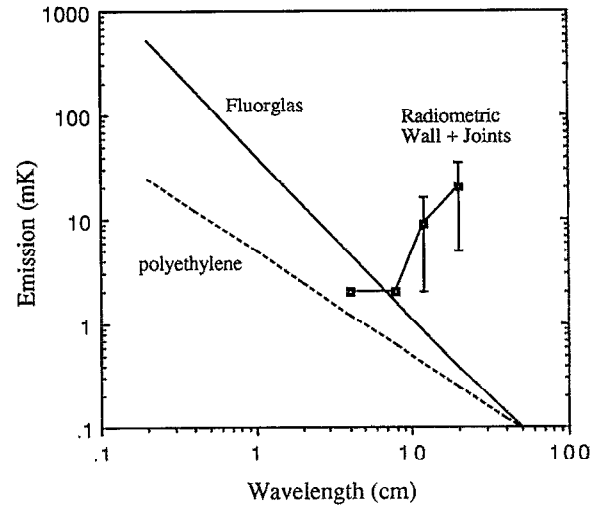

FIG. 6. Emission from windows and radiometric wall. Values are for the observed radiometric wall temperature profile. The upper and lower IR-blocking windows are at 50 ± 10 and 25 ± 10 K, respectively; the polyethylene windows are at 250 ± 10 K. The radiometric wall data are calculated.

VII. COLD LOAD RADIOMETRIC TEMPERATURE

We evaluate the radiometric temperature of the cold load for the four radiometers used at the South Pole in 1989 (see Table VI). A similar procedure would be used to calculate the radiometric temperature for other instruments. The ambient barometric pressure during the CMB measurements at the South Pole ranged from 516 to 523 Torr. The barometric pressure over the LHe bath is increased by 1.0 ± 0.1 Torr due to the LHe boiloff and by <0.1 Torr due to the weight of the column of cold He gas. The uncertainty in the barometric pressure over the LHe bath during any given measurement was ±1 Torr, dominated by the uncertainty in the measurement of the ambient pressure. The 517–524-Torr pressure over the LHe bath corresponded to a thermodynamic temperature of 3.835 to 3.847 K (Ref. 30) with an uncertainty during any given measurement of ±0.002 K.

The correction to the absorber temperature due to reflection is obtained from the calculation of r^2 in Appendix A. The reflection correction, $T_{\rm refl}$, can be expressed in the form of Eq. (6). In terms of the radiometer reflection coefficient, r_R, and the effective load reflection coefficient, $r_{\rm CL}$:

$$T_{\rm refl}=(T_B-T_{A,\rm abs})[\,|r_{\rm CL}|^2+r_{\rm CL}r_R\cos(\Delta\phi)\,], \qquad (7)$$

where $\Delta\phi$ is the phase difference between the load reflection and radiometer reflection. We refer to the first term of Eq. (7) as the incoherent reflection and the second term as the coherent reflection.

The incoherent reflection is the sum of the power reflections and coherent reflections from within the load; the error is equal to the quadrature sum of the individual errors (see Table II). The coherent reflection is the sum of reflections dependent on radiometer position. The mean value of the coherent reflection is zero because the phase is unknown. We estimate the error as the linear sum of the rms of each of the coherent reflection terms (see Tables II and V). This is a more conservative estimate than the quadrature sum.

The temperatures of the upper and lower IR-blocking windows are 50 ± 10 K and 25 ± 10 K, respectively (see

TABLE VI. Cold load antenna temperature. The values are for the four radiometers which used this load at the South Pole in Dec. 1989. The absorber leakage is included in the wall emission. The pressure over the LHe bath was 520 Torr, corresponding to a thermodynamic temperature of 3842 mK. $T_{A,\rm CL}$ is the absorber emission plus the total correction.

	Signal			
Source	20 cm (mK)	12 cm (mK)	7.9 cm (mK)	4.0 cm (mK)
Window emission	1 ± 1	1 ± 1	2 ± 1	6 ± 2
Radiometric wall emission	24 ± 16	10 ± 7	2 ± 2	2 ± 2
Incoherent reflection	23 ± 15	7 ± 4	6 ± 5	7 ± 9
Coherent reflection	0 ± 8	0 ± 5	0 ± 18	0 ± 13
Total correction to absorber emission	48 ± 23	18 ± 10	10 ± 18	15 ± 16
Absorber emission	3806 ± 2	3782 ± 2	3752 ± 2	3665 ± 2
Cold load antenna temperature, $T_{A,\rm CL}$	3854 ± 23	3801 ± 10	3762 ± 19	3679 ± 16

Sec. VIII B). Their emission (see Table IV and Fig. 6) is obtained using the emissivity from Sec. VI B.

The wall temperature increases from 50 K just above the IR-blocking windows to 120 K where the He boiloff gas enters the vent tubes (25 cm from the mouth) to 250 K (ambient temperature during the measurements) at the load aperture. At $\lambda = 7.9$ and 4.0 cm, the wall contribution is estimated from the convolution of the antenna beam with the wall emission (Sec. IV E). At $\lambda = 20$ cm, where the free-space approximation is poor, we calculate the loss[31] for each of the 16 waveguide modes which can propagate. The amplitude of each mode is given by the mode-conversion calculation described in Appendix B. We estimate the contribution due to the joints in the wall in the ray approximation and use the amplitude of the emission as the uncertainty to account for modeling uncertainties. The wall emission at 12 cm is interpolated from the 20- and 7.9-cm values (see Fig. 6).

Radiation from the annular space between the radiometric wall and the dewar wall may leak into the radiometric space through the absorber due to improper rf sealing around the absorber. The blackbody temperature of the annular space is 15 ± 10 K warmer than the LHe bath and thus can increase the radiometric temperature of the absorber. Roughly $50 \pm 25\%$ of the signal enters into the absorber, and $\sim 1.0 \pm 0.5\%$ of the signal passes through the absorber at $\lambda = 20$ cm. The effective gain-weighted radiating surface is $\sim 9\%$ of the total absorber area. The total contribution at $\lambda = 20$ cm is 7 ± 8 mK. The absorber attenuation scales exponentially with $1/\lambda$, and the effect is < 1 mK for $\lambda < 15$ cm.

VIII. THERMAL PERFORMANCE

A. Liquid-helium loss rate

In the absence of the IR-blocking windows, the principal heat leak to the liquid helium bath would be radiative. During a calibration, the heat leak would be of order 30 W; between calibrations, when the load is uncovered, the heat leak would be of order 100 W. We calculate the radiative heat leak with the IR-blocking windows, Q_R, from measurements of the transmission of the Fluorglas window material at 300 and 4.2 K over the 100–1000-cm^{-1} range using a Fourier spectrometer. The measurements indicate that three layers at 300 K (4.2 K) transmit only 2% (5%) of the power. Assuming a 250-K greybody with emissivity $e \sim 0.3$ at the load aperture with the IR-blocking windows at 20–50 K (similar to the $\lambda = 20$-cm antenna observing the load), we predict a radiative heat leak to the LHe bath of $0.6 < Q_R < 1.6$ W.

We can also estimate Q_R from the difference in the total heat leak to the helium bath during calibration with the 20-cm wavelength radiometer (3.1 W) and the total heat leak with the low-emissivity cover in place (2.2 W). The cover ($e \sim 0.05$) emits $\leqslant 0.25$ W at 250 K, much less than the radiometer antenna. The heat leak difference is approximately equal to the radiative component: $Q_R \sim 0.9$ W, consistent with our predictions.

The remaining heat leak to the LHe bath of 2.2 W comes primarily from conduction down the dewar and radiometric walls. In the absence of any vapor cooling, the conductive heat leak would be ~ 9 W. The heat leak through the dewar vacuum space is < 0.1 W. The convective and conductive heat leak down the He gas column is < 0.1 W with the IR-blocking windows in place.

B. Infrared-blocking window temperature

The boiloff gas exits the load at a temperature of ~ 120 K when the aperture is covered by the 20-cm wavelength radiometer antenna (the maximum radiative heat leak). From the LHe loss rate and the enthalpy of the exiting boiloff gas, we calculate that the gas removes ~ 88 W of thermal power from the load. While the radiative heat load to the LHe bath is only ~ 3 W, the ~ 35-K temperature drop across the IR-blocking windows (see Sec. VII) indicates that ~ 30 W of radiant and convective power is absorbed. The remaining ~ 58 W removed is primarily from vapor cooling of the dewar and radiometric walls.

The heat load to the upper (lower) IR-blocking window is < 6 (< 1.5) mW cm^{-2}. Because the heat loading to both windows is small and the boiloff gas is in good contact with the windows, the windows and boiloff gas are in thermal equilibrium. The radiometric wall, measured to be 50 K just above the IR-blocking windows and 15 K just below, is also in good thermal equilibrium with the boiloff gas. We infer that the upper and lower IR-blocking windows are at 50 ± 10 K and 25 ± 10 K, respectively. The uncertainties take into consideration the efficiency of the convective vapor cooling and possible radiative heating.

IX. OPERATIONAL PERFORMANCE

We prepared the cold load for operation by flushing it with nitrogen gas at a slow rate, changing the volume of gas ~ 14 times and heating the interior to ~ 30 °C. We then filled the load with liquid nitrogen to precool it. After several hours, the liquid was pumped out through the fill line at a rate of ~ 1 ℓ/min and residual liquid in the bottom of the curved dewar was boiled off with the heater. The load was then purged of the nitrogen gas by flowing ~ 7 times the load volume of He gas into the top of the load while pulling out the colder, heavier nitrogen gas via the fill line. As an added precaution, He gas was flowed in the fill line and through the entire system, including the pressure sensing lines.

After a ~ 15 min initial cooldown period, LHe could be transferred at a rate of 3.6 ℓ/min (~ 0.7 cm/min). The load was filled to 15–20 cm above the absorber tips, sufficient for a full day of observations. During observations, the level dropped by $\leqslant 0.85$ cm/h and the pressure above the LHe bath was < 1 Torr above ambient. The top window was periodically checked for frost or debris and cleaned if necessary.

TABLE VII. Comparison of cold loads used for long-wavelength measurements of the CMB. Characteristics are given at the wavelength of each measurement. r^2 is the incoherent (power) reflection coefficient (including any correction for illumination). T_B is the radiometer broadcast temperature. Subscripts RW and W designate the radiometric wall and windows, respectively. The total correction to the LHe bath temperature is given by T_{CORR}. Values for "This work" are from Table VI. When the design required a break in the horn, or when the cold load and sky signals reached the radiometer following different paths, the correction for antenna emission is given by T_{Horn}.

Measurement	λ (cm)	r^2 (10^{-4})	r^2T_B (mK)	$e_{RW}T_{RW}$ (mK)	e_WT_W (mK)	T_{CORR} (mK)	T_{Horn}[a] (mK)
Sironi *et al.* 1990[b]	50	13±3	455±105	1450±280	0	1900±300	1550±130
Sironi *et al.* 1990[b]	12	28±3	140±15	4760±300	0	4800±300	26780±500
This work	20	5.2	26±19	24±16	1±1	48±29	···
This work	12	1.5	7±2	10±7	1±1	18±14	···
This work	7.9	0.5	7±4	2±2	2±1	10±24	···
This work	4.0	0.5	13±8	2±2	6±2	15±18	···
Stokes *et al.* 1967[c]	3.2	6±3	20±10	160±100	60±20	240±100	[d]
Stokes *et al.* 1967[c]	1.58	10±3	30±10	210±80	40±10	280±80	3
Wilkinson 1967[c]	0.856	0±3	0±10	280±110	60±60	340±125	···
Johnson and Wilkinson 1987[e]	1.2	5	0±18[f]	0	35±12[g]	35±22	50±12

[a](···) indicates that the calibration was at the horn aperture.
[b]Coaxial cold load used is that described in Limon *et al.* 1989. These measurements were conducted in 1988 at Alpe Gera, Italy. The 12-cm wavelength radiometer, the same instrument as that used in "This work," is capable of using either load.
[c]The measurements at 3.2, 1.58, and 0.856 cm used the same cold load.
[d]No value for this quantity is given.
[e]The cold load is an integral part of the radiometer.
[f]Difference in horn and load reflection using conservative error bars added in quadrature.
[g]Window is viewed during sky observation and not during cold load calibration.

X. COMPARISON WITH OTHER COLD LOADS

Coaxial cold loads used in the past have typically had ~300-mK error, even in the same wavelength range as this quasi-free-space cold load. Previous quasi-free-space cold loads (excepting the 1982 load) have had larger corrections to the LHe bath temperature and larger uncertainties in the resulting $T_{A,CL}$ than this load. Table VII compares four cold loads used for CMB measurements over the range from ~1–50-cm wavelength. The measurement at 50 cm is that of Sironi *et al.*[32]

The 12- and 7.9-cm wavelength radiometers have made measurements using both the 1982 and 1988 cold loads[3,4,7,33,34] and these measurements serve as cross checks between the two loads. The uncertainties are large compared to the uncertainty quoted in this work because of uncertainties in the atmospheric correction (~±50 mK), so a comparison at the level of the quoted uncertainties on $T_{A,CL}$ is not possible with the existing data.

Table VIII summarizes the predicted load temperature, $T_{A,CL}$, and the measured temperatures of the atmosphere, $T_{A,Atm}$, and CMB, $T_{A,CMB}$ at 7.9-cm wavelength from 1986–9. The weighted averages of $T_{A,CMB}$ agree: for 1988–9 the result is 97±102 mK higher than for 1986–87. The largest contribution to the error in this CMB measurement is the correction for atmospheric emission. For the three measurements made at White Mountain (1986–88), $T_{A,CMB} + T_{A,atm}$ is 191±58 mK hotter as measured with the 1988 cold load, whereas $T_{A,atm}$ is measured to be only 64±84 mK hotter in 1988.

Any increase from 1986–7 to 1988–9 due to the load used implies a decrease in the true cold load antenna temperature (when compared to the calculated $T_{A,CL}$) from the 1982 load to the 1988 load. If due to the 1988 load, this would require a significant negative coherent reflection correction to the LHe bath temperature (predicted to be less than 18 mK in magnitude). The 1982 load could be warmer than predicted if the radiometric properties changed due to repeated use and/or the wall emission was underestimated. Another potential source of emission which was unaccounted for in the 1982 load is from the antenna/load interface which did not dc-isolate the antenna and load. The difference in the measured CMB temperature could also be due to errors in the measurement of contributions to the sky signal. For example, the CMB

TABLE VIII. Comparison of CMB measurements made with the 1982 and 1988 cold loads.

Year	1986	1987	1988	1989
Observing site	White Mountain	White Mountain	White Mountain	South Pole
λ (cm)	8.1[a]	7.9	7.9	7.9
Load used	1982	1982	1988	1988
Predicted $T_{A,CL}$	3735± 55	3742±38	3697±21	3762±19
$T_{A,Atm}$	870±108	898±64	955±55	1109±60
$T_{A,CMB}$	2580±130	2460±79	2621±65	2549±74

[a]Radiometer center wavelength was changed from 8.1 cm in 1986 to 7.9 in 1987; the bandwidth was also reduced, from 460 to 200 MHz, which increased the amplitude of the coherent reflection terms for this radiometer.

difference could be explained if the atmospheric signal were 97 mK warmer than measured in 1988–9 (or cooler than measured in 1986–87).

We conclude that the differences in data obtained using the 1982 and 1988 loads are not significantly different, but that they do suggest one of the following: (1) the 1982 load is warmer than reported (or the 1988 load is cooler than reported), (2) the 7.9-cm wavelength radiometer had an offset (or other correction to the data) which was dependent on both the cold load and the radiometer position, or (3) the atmosphere was warmer than measured in 1988.

XI. POSSIBLE IMPROVEMENTS

The back of the absorber should be completely closed, allowing no path for radiation to enter from outside the radiometric wall. The joints in the wall should be covered or eliminated. The glass–Teflon IR-blocking material would perform better both in the IR and microwave if the glass were quartz and if, instead of a woven fabric, the glass were a thin film. Any future CMB spectrum measurement should include direct measurements of the reflection from the radiometer antenna, the radiometer/load interface plate and the load, similar to those made with the 20-cm wavelength radiometer.

This cold load could be used at $\sim$30-cm wavelength if a thicker absorber were used. To be useful at wavelengths much greater than 30 cm, careful radiometric analysis and testing of the load would be required (in addition to the use of a correspondingly thicker absorber). If the wall diameter and absorber thickness are simply scaled with wavelength, the volume of LHe required to begin operation ($\propto\lambda^3$) and the loss rate ($\propto\lambda^2$) increase rapidly, making the quasi-free-space design impractical for very long-wavelength calibration. To be useful at shorter wavelengths ($\lambda<2.5$ cm), a better IR-blocking material should be used or a higher heat leak to the LHe bath must be tolerated. The corrections due to window and wall emission would be reduced if the calibration were done at balloon altitude, where these emissive parts of the calibrator could be operated at lower temperatures.[35]

ACKNOWLEDGMENTS

We thank John Gibson for the electronics in the cold load, the Mechanical Shops at the Lawrence Berkeley Laboratory, in particular Armando Meuti and Kit Mui for their help in manufacturing parts of the load, Keith Alexander at Kadel Engineering, David Miller and Bob McMurray of UC Berkeley for their help in measuring the IR properties of Fluorglas, and Scott Friedman for work on the 1982 load. We also gratefully acknowledge the assistance of Barron Chugg, Jenny Hwang, Jay Levin, Michele Limon, and Faye Mitschang. This work was supported by the National Science Foundation Division of Polar Programs under Contract No. DPP-8716548, the Physics Division of the Lawrence Berkeley Laboratory, and the Division of High Energy Physics of the U.S. Department of Energy under Contract No. DE-AC03-76SF00098.

APPENDIX A: COLD LOAD REFLECTION

The radiometer broadcast power, with electric field amplitude E_0, is reflected by the absorber, the LHe surface, the windows, the cold load interface, and in the radiometer itself, resulting in reflected power with electric field amplitude E_r. The ith component of the reflected signal has an amplitude $E_0 r_i$ and phase ϕ_i which is related to the phase of the reflection internal to the radiometer (taken as the reference phase). Neglecting multiple reflections, the amplitude reflection coefficient, r, is the sum:

$$r=E_r/E_0=r_R+r_I e^{i\phi_I}+r_{P1}e^{i\phi_{P1}}+r_{P2}e^{i\phi_{P2}}+r_{F1}e^{i\phi_{F1}}+r_{F2}e^{i\phi_{F2}}+r_H e^{i\phi_H}+r_A e^{i\phi_A}, \tag{A1}$$

where the subscripts R, I, P, F, H, and A refer to the radiometer, the antenna/load interface, the polyethylene, the IR-blocking windows (made of Fluorglas), the LHe surface, and the absorber. The polyethylene windows have equal thickness ($r_{P1}=r_{P2}$); the lower IR-blocking window has twice the thickness of the upper ($r_{F2}=4r_{F1}$). The antenna/load interface term is generally predicted to be very small ($r\approx 3\times10^{-3}$ for the 20-cm wavelength radiometer; see Appendix B) and the term for radiometer/load interface reflection is dropped. The LHe surface reflection is given by $r_H=(\epsilon_{\rm LHe}-\epsilon_{\rm He})/(\epsilon_{\rm LHe}+\epsilon_{\rm He})=1.0\times10^{-2}$.

To find the correction due to reflection we compute $|r|^2$:

$$\begin{aligned}|r|^2=&r_R^2+2r_P^2+r_{F1}^2+r_{F2}^2+r_H^2+r_A^2+2r_R r_P\cos(\phi_{P1})+2r_R r_P\cos(\phi_{P2})+2r_R r_{F1}\cos(\phi_{F1})+2r_R r_{F2}\cos(\phi_{F2})\\&+2r_R r_H\cos(\phi_H)+2r_R r_A\cos(\phi_A)+2r_P^2\cos(\phi_{P1}-\phi_{P2})+2r_{F1}r_{F2}\cos(\phi_{F1}-\phi_{F2})+2r_{F1}r_H\cos(\phi_{F1}-\phi_H)\\&+2r_{F1}r_A\cos(\phi_{F1}-\phi_A)+2r_{F2}r_H\cos(\phi_{F2}-\phi_H)+2r_{F2}r_A\cos(\phi_{F2}-\phi_A)+2r_H r_A\cos(\phi_H-\phi_A).\end{aligned} \tag{A2}$$

The r_R^2 term is a correction to the radiometer gain and broadcast temperature and does not affect the cold load temperature or the measurement.

The reflection dilution factor D, calculated in the ray approximation, is the fraction of power broadcast which reenters the antenna aperture. This factor applies to all terms and for the longest wavelength radiometers, $D\sim1$.

The phase-dependent terms represent signals reflected from two points arriving at the first amplifier with correlated phases. The path length between two sources a and b, $2x_{a,b}$, and the radiometer bandwidth, $\Delta\nu$, determine the degree of coherence, C:

$$C(z_{a,b})=\left(\frac{\sin(z)}{z}\right)^2 \quad \text{for} \quad z<\frac{\pi}{2}$$
$$\approx\left(\frac{1}{z}\right)^2 \quad \text{for} \quad z>\frac{\pi}{2}, \tag{A3}$$

where $z_{a,b}=2\pi x_{a,b}/L$, $L=c/\Delta\nu$ is the coherence length of the signal, and c is the speed of light, and we assume a square bandpass.

The cold load reflection coefficient is:

$$\begin{aligned}|r|^2=&2r_P^2+r_{F1}^2D_{F1}+r_{F2}^2D_{F2}+r_H^2D_H+r_A^2D_A+2r_Rr_{P1}\cos(\phi_{P1})C(z_{R,P1})+2r_Rr_{P2}\cos(\phi_{P2})C(z_{R,P2})\\&+2r_Rr_{F1}\cos(\phi_{F1})D_{F1}C(z_{R,F1})+2r_Rr_{F2}\cos(\phi_{F2})D_{F2}C(z_{R,F2})+2r_Rr_H\cos(\phi_H)D_HC(z_{R,H})\\&+2r_Rr_A\cos(\phi_A)D_AC(z_{R,A})+2r_{F1}r_{F2}\cos(\phi_{F1}-\phi_{F2})D_{F1}C(z_{F1,F2})+2r_{F1}r_H\cos(\phi_{F1}-\phi_H)D_{F1}C(z_{F1,H})\\&+2r_{F1}r_A\cos(\phi_{F1}-\phi_A)D_{F1}C(z_{F1,A})+2r_{F2}r_H\cos(\phi_{F2}-\phi_H)D_{F2}C(z_{F2,H})+2r_{F2}r_A\cos(\phi_{F2}-\phi_A)D_{F2}C(z_{F2,A})\\&+2r_Hr_A\cos(\phi_H-\phi_A)D_HC(z_{H,A})+2r_P^2\cos(\phi_{P1}-\phi_{P2})D_{P1}C(z_{P1,P2}).\end{aligned} \tag{A4}$$

The first five terms in Eq. (A4) are phase-independent terms and are calculated from measured and predicted reflection coefficients. Terms 6–11 are coherent reflection terms dependent on the distance between the radiometer and the load and are proportional to the reflection coefficient of the radiometer. The radiometer/load phase difference is unknown, so our best estimate of these terms is zero with an error equal to the rms. We use the linear sum of these terms to estimate the magnitude of the position-dependent reflection effect. This estimate of the error due to these coherent reflection terms is conservative because we have used the linear sum whereas some of the terms could partially cancel each other. Note that each term in the sum has a large uncertainty due to our poor knowledge of r_R. We estimate the error in r_R as $+100\%/-50\%$.

The last seven terms (12–18) are coherent reflection terms dependent on the separations between the reflecting surfaces within the load. Because they are independent of radiometer position, we group these terms with the incoherent reflection terms. The IR-blocking window separation is known to ± 1 cm, so the phase difference in term 12 is known. Our best estimate of this term is included as a correction and $\pm 50\%$ of this term is included in the calculation of the uncertainty in the incoherent reflection.

The last six terms (13–18) depend on separations which are not well known. The phases of the polyethylene window reflection and the LHe surface reflection vary during calibration. We have no knowledge of the phase of the reflection from the absorber. We average over the unknown phases and take the quadrature sum of terms 13–18 as a contribution to the incoherent reflection uncertainty. For the radiometers used at the South Pole in 1989, Table IX shows some of the radiometer parameters which enter into Eq. (A4) and Table II shows the values of the resulting terms.

APPENDIX B: ANTENNA/COLD LOAD INTERFACE REFLECTION

The term for antenna/load reflection in Appendix A is taken to be negligible and dropped to simplify the calculation of the load reflection. That approximation is based on an analysis of the matching between the pyramidal, E-plane corrugated antenna of the 20-cm wavelength radiometer and the load. At the long-wavelength limit of the operating range, the approximation to free space is poor, interface reflections should be largest, and the interface reflection is most difficult to measure.

We model the antenna-load interface by an interface from E-plane corrugated rectangular waveguide to circular guide and calculate the mode conversion. This approximates the 19°-flare horn antenna by a straight waveguide with only the $HE_{1,2}$ fundamental mode propagating.[36] The $HE_{1,2}$ field distribution at the interface is matched to the 16

TABLE IX. Radiometer-dependent reflection coefficient parameters in Eq. (A4). r_R^2 has a factor of 2 uncertainty. For reflection dilution factors, $D_A\sim D_H$ and $D_F\equiv D_{F1}\sim D_{F2}$. The coherence factor $C(z_{F1,F2})\sim 1$ and average values are given for terms like $C(z_{R,H})$ which depend on the LHe level.

Quantity	Units	Value			
		20 cm	12 cm	7.9 cm	4.0 cm
r_R^2		0.01	0.01	0.1	0.01
L	(cm)	150	187	150	60
$T_F T_{abs}$	(K)	50	27	86	279
D_F		1	1	0.46	0.079
D_H		1	1	0.23	0.050
$C(z_{R,F})$		0.044	0.045	0.026	0.0074
$C(z_{R,H})$		0.025	0.028	0.017	0.0042
$C(z_{F,H})$		0.44	0.60	0.44	0.071
$C(z_{F,A})$		0.22	0.34	0.22	0.035
$C(z_{H,A})$		0.87	0.92	0.87	0.39

modes with cutoff wavelengths above 20 cm for the 78-cm radiometric wall diameter. The amplitudes are determined by calculation of overlap integrals and requiring energy conservation.[37,38] The results show that the $HE_{1,2}$ mode matches very well to the circular guide: the rectangular mode amplitude reflection coefficients are all $<5\times10^{-3}$ and the amplitude reflection of the fundamental is 3×10^{-4}. The modes launched into the circular guide have amplitudes which decrease rapidly with increasing mode number.

The 12-cm wavelength radiometer antenna is based on the same design as the 20-cm wavelength antenna and the shorter wavelength should give a better match. At shorter wavelengths, the free-space approximation is better and we measure the difference in antenna/load and antenna/sky interface power reflection by placing the transition plate over the antenna and observing the signal change. These tests are consistent with no effect at the 25-mK level at 4-cm wavelength.

While antenna/load interface effects seem to be small, further study of differences in sky and load reflections should be undertaken. Here, we take this effect to be negligible and, because it is very instrument-dependent, we do not include it in the load analysis.

[1] G. Smoot *et al.*, Phys. Rev. Lett. **51**, 1099 (1983).
[2] A. Kogut, M. Bensadoun, G. De Amici, S. Levin, G. F. Smoot, and C. Witebsky, Astrophys. J. **355**, 102 (1990).
[3] G. De Amici, M. Bensadoun, M. Bersanelli, A. Kogut, S. Levin, G. Smoot, and C. Witebsky, Astrophys. J. **359**, 219 (1990).
[4] G. Sironi, G. Bonelli, and M. Limon, Astrophys. J. **378**, 550 (1991).
[5] M. Bensadoun, M. Bersanelli, G. De Amici, A. Kogut, M. Limon, S. Levin, G. F. Smoot, and C. Witebsky, Astrophys. J. (submitted, 1992).
[6] S. Levin, M. Bensadoun, M. Bersanelli, G. De Amici, A. Kogut, S. Levin, M. Limon, and G. Smoot, Astrophys. J. (submitted, 1992).
[7] G. De Amici, M. Bensadoun, M. Bersanelli, A. Kogut, S. Levin, M. Limon, and G. Smoot, Astrophys. J. **381**, 341 (1991).
[8] This measures power in units of antenna temperature T_A which is related to the thermodynamic temperature T of the source by $T_A=Tx(e^x-1)^{-1}$, where $x=h\nu/kT$. Over the operating range of the CL, $T_A\approx T$.
[9] A. Kogut, M. Bensadoun, M. Bersanelli, G. De Amici, S. Levin, M. Limon, and G. Smoot, in *AIP Conf. Proc. 222: After the First Three Minutes*, edited by S. Holt, C. Bennet, and V. Trimble (American Institute of Physics, New York, 1991), p 62.
[10] A. A. Penzias, IEEE Trans. Microwave Theory Tech. **MTT-16**, 608 (1968).
[11] M. Limon, C. Marchioni, and G. Sironi, J. Phys. E (UK) **22**, 963 (1989).
[12] For a review of CMB measurements up to 1980, see R. Weiss, Ann. Rev. Ast. Astrophys. **18**, 489 (1980).
[13] R. A. Stokes, R. B. Partidge, and D. T. Wilkinson, Phys. Rev. Lett. **19**, 1199 (1967).
[14] M. S. Ewing, B. F. Burke, and D. H. Staelin, Phys. Rev. Lett. **19**, 1251 (1967).
[15] D. T. Wilkinson, Phys. Rev. Lett. **19**, 1195 (1967).
[16] C. Witebsky, Ph. D. Thesis, Dept. of Astronomy, U.C. Berkeley (1985).
[17] G. Smoot *et al.*, Astrophys. J. Lett. **291**, L23 (1985).
[18] G. F. Smoot, M. Bensadoun, M. Bersanelli, G. De Amici, A. Kogut, S. Levin, and C. Witebsky, Astrophys. J. Lett. **317**, L345 (1987).
[19] M. Bersanelli, C. Witebsky, M. Bensadoun, G. De Amici, A. Kogut, L. Levin, and G. Smoot, Astrophys. J. **339**, 632 (1989).
[20] A. Kogut, M. Bersanelli, G. De Amici, S. D. Friedman, M. Griffith, B. Grossan, S. Levin, G. F. Smoot, and C. Witebsky, Astrophys. J. **235**, 1 (1988).
[21] Eccosorb is manufactured by Emerson & Cuming, Canton, MA.
[22] J. D. Jackson, *Classical Electrodynamics*, 2nd ed. (Wiley, New York, 1975), pp. 286–287.
[23] G. Sironi (private communication, 1988).
[24] S. Ramo, J. R. Whinnery, and T. Van Duzer, *Fields and Waves in Communication Electronics* (Wiley, New York, 1965), p. 351.
[25] Manufactured by Fluorglas, a division of Allied Signal.
[26] Teflon is manufactured by E.I. DuPont de Nemours & Co., Inc., Wilmington, DE.
[27] S. Ramo, J. R. Whinnery, T. Van Duzer, *op. cit.*, p. 288.
[28] J. Bardeen, J. Appl. Phys. **11**, 88 (1940).
[29] M. Halpern, H. P. Gush, E. Wishnow, and V. De Cosmo, Appl. Opt. **25**, 565 (1986).
[30] M. Duriex and R. L. Rusby, Metrologia **19**, 67 (1983).
[31] S. Ramo, J. R. Whinnery, and T. Van Duzer, *op. cit.*, p. 434.
[32] G. Sironi, M. Limon, G. L. Marcellino, G. Bonelli, M. Bersanelli, G. Conti, and K. Reif, Astrophys. J. **378**, 550 (1991).
[33] G. Sironi and G. Bonelli, Astrophys. J. **311**, 418 (1986).
[34] G. De Amici, G. Smoot, J. Aymon, M. Bersanelli, A. Kogut, S. Levin, and C. Witebsky, Ap. J., **329**, 556 (1988).
[35] D. G. Johnson and D. T. Wilkinson, Astrophys. J. Lett. **313**, L1 (1986).
[36] C. Witebsky, G. F. Smoot, S. Levin, and M. Bensadoun, IEEE Trans. Antennas Propag. **AP-35**, 1310 (1987).
[37] A. Wexler, IEEE Trans. Microwave Theory Tech. **MTT-15**, 508 (1967).
[38] M. S. Narasimhan and V. Venkateswara Rao, IEEE Antennas Propagation, **AP-21**, 320 (1973).